BCS theory has to be overhauled: reassurance from numerical survival rate

Zheng, X. H., & Walmsley, D. G. (2016). BCS theory has to be overhauled: reassurance from numerical survival rate. *Solid state communications*, *237-238*, 42-48. https://doi.org/10.1016/j.ssc.2016.03.026

Published in:
Solid state communications

Document Version:
Peer reviewed version

BCS theory has to be overhauled: reassurance from numerical survival rate

X. H. Zheng and D. G. Walmsley
*Department of Physics and Astronomy, Queen's University of Belfast, BT7 1NN, N. Ireland**
(Dated: February 22, 2017)

The BCS theory has conceptual and numerical difficulties. We have previously overhauled it with a new scheme of phonon-mediated electron pairing that can be expressed analytically in terms of an empirical pairing survival rate factor, $S(\mathbf{q}) = 0$ or $1/2$, depending on phonon momentum, $\mathbf{q}$. Now we evaluate $S(\mathbf{q})$ numerically entirely from experimental data on normal state electrical resistivity and on superconducting tunnelling conductance. The empirical and numerical $S(\mathbf{q})$ are reassuringly close in aluminium and lead and particularly so in two other cases, niobium and tantalum.

PACS numbers: 71.15.Dx, 74.25.Kc, 31.10.+z

I. INTRODUCTION

For nearly 60 years the theory of Bardeen, Cooper and Schrieffer (BCS) has been universally accepted as providing the best microscopic description of conventional superconductivity [1]. However, uncomfortable signs of strain, both conceptual and numerical, have kept emerging to question the validity of the theory [2]. The problem conceptually is that the theory doubly and contradictorily defines electron pair occupancy probabilities when the electrons from normal and umklapp scattering processes compete for the same destination state [3, 4]. Numerically, attempts to calculate superconducting properties with the BCS theory from first principles have always been to varying degrees less than successful. For example the calculated value of the superconducting transition temperature, T_c, is found to be persistently too high when calculated values of the normal state electrical resistivity against temperature, $\rho(T)$, are reasonable. Conversely but equivalently, when T_c from calculation is reasonable, $\rho(T)$ is found to be too low [5–18].

Previously we found an empirical modification to overhaul the BCS theory: disallow pairing when normal and umklapp scattering processes terminate in the same state. It can be expressed analytically in terms of a pairing survival rate factor, $S(\mathbf{q}) = 0$ or $1/2$, depending on whether or not the phonon momentum, $\mathbf{q}$, invokes both normal and umklapp scattering. Encouragingly this scheme, designed to circumvent the conceptual issue in BCS, also eases the numerical difficulty. Now the numerical value of T_c is reduced when reasonable values of $\rho(T)$ are implemented. It turns out that the introduction of the empirical $S(\mathbf{q})$ settles the BCS numerical issue in the cases of lead, aluminium, niobium and tantalum with high accuracy [3, 4] as it does too in tungsten, iridium, molybdenum and vanadium [19, 20].

Considering the long established status of the BCS theory, we here seek as reassurance a numerical specification of $S(\mathbf{q})$. Starting from the empirical configuration $S(\mathbf{q}) = 0$ or $1/2$ previously asserted we allow its value to vary arbitrarily as long as the fit between theory and experiment improves in the superconducting state. While doing so we retain the exact strength of the electron-phonon interaction found in the normal state without change. Previously, in contrast, we merely demonstrated its consistency with the interaction strength in the superconducting state [3, 4].

Specifically we invert values of experimental $\rho(T)$ to determine the electron-phonon interaction strength in the normal state in the form of a numerically well-defined atomic pseudopotential, $V(r)$, which if left unmodified leads to excessively strong superconductivity, a result consistent with the overwhelming historical evidence. This process involves no questionable physical theory or uncontrolled computational errors. By way of modification, we transform $V(r)$ into $V(\mathbf{q})$ in reciprocal space and replace $V^2(\mathbf{q})$ with $S(\mathbf{q})V^2(\mathbf{q})$ in the relevant formulation. Then we let computational calculation determine the values of $S(\mathbf{q})$ automatically, as we aim to regenerate the experimental tunnelling conductance data in the superconducting state. We are reassured to observe the empirical $S(\mathbf{q})$ reemerging from the largely free-running machine procedure surprisingly well particularly in the cases of the metals niobium and tantalum.

This article is arranged as follows. In Section II we review the evidence that led to the proposed scheme to overhaul the BCS theory. In Section III we consider a specific case, lead, and obtain an accurate Born-von Karman model for phonon dispersion a task that defied many previous attempts but is crucial for a successful implementation of the BCS theory and its possibly improved version. In Section IV we determine the strength of the electron-phonon interaction in lead. In Section V we introduce the numerical scheme that overhauls the BCS theory and numerically determines $S(\mathbf{q})$. In Section VI we study further cases: aluminium, niobium and tantalum. Brief discussion and conclusions are in Sections VII and VIII.

II. HISTORICAL BACKGROUND

In the normal state $\rho(T)$ arises from the electron-phonon interaction that in turn can be regarded as aris-

*Electronic address: dg.walmsley@qub.ac.uk

ing from $V(r)$, where r stands for the distance from the atomic site. In the Eliashberg-Nambu formalism, a refined version of the BCS theory, the superconducting energy gap arises from the electron-phonon spectral density, $\alpha^2F(\nu)$, that also derives from $V(r)$ [21]. It is natural to expect that we can find both $\rho(T)$ and $\alpha^2F(\nu)$ via first principles calculations with a consistent $V(r)$. Unfortunately each and every previous attempt in this direction has failed, leaving us with a long trail of evidence in the literature of an unresolved difficulty.

In an early example, Tomlinson and Carbotte [5] in 1976 evaluated $\alpha^2F(\nu)$ for lead with the pseudopotential of Appapillai and Williams which is a particular specification of the Heine-Abarenkov potential. Ostensible agreement with tunnelling measurement was considered to be "very good", although the longitudinal numerical peak of the spectral function $\alpha^2F(\nu)$ at 9 meV is more than 2 times stronger than the observed tunnelling peak [21]. Soon after, in 1977 Tomlinson and Carbotte [6] evaluated the normal state resistivity $\rho(T)$ for lead with the same potential. Between $T = 4$ and 295 K their $\rho(T)$ is about 75% of the observed values, as can be seen more clearly from the graphic portrayal of the result in 1981 by Eiling and Schilling (see upper part of FIG. 2) [7]. A similar discrepancy occurred when aluminium was investigated using the Heine-Abarenkov potential tabulated by Harrison (where the discrepancy in ρ was somewhat obscured by a logarithmic presentation) [8–10].

In 1977 Peter, Ashkenazi and Dacorogna studied the effects of anisotropy on the T_c of niobium [11]. Intriguingly they found that the electron-phonon coupling constants determined are probably too large and have to be multiplied by a factor of 0.7 (which means a factor of 0.49 in the electron-phonon-electron interaction) in order to obtain the observed T_c.

In 1979 Glötzel, Rainer and Schober [12] evaluated $\alpha^2F(\nu)$ for vanadium, niobium, tantalum, molybdenum, tungsten, palladium, platinum and lead. They carefully avoided any uncontrolled approximations. To find phonon dispersion they used published Born-von Karman fits to the force constants. To estimate the strength of the electron-phonon interaction they used muffin-tin potentials developed for band structure calculations. The superconducting transition temperature they found, T_c, turns out to be 2 to 3 times too high. They show the value of the Coulomb pseudopotential, μ^*, has a significant effect on T_c but stick to a reasonable choice $\mu^* = 0.13$. They conclude that their careful approach was incapable of reproducing the observed values of T_c.

In 1987 Al-Lehaibi, Swihart, Butler and Pinski [13] evaluated both $\rho(T)$ and $\alpha^2F(\nu)$ for tantalum also with a muffin tin potential from band calculation. While $\rho(T)$ was found to be slightly lower than experimentally observed, $\alpha^2F(\nu)$ exceeded the tunnelling values significantly, giving $T_c = 7.01$ K (4.5 K experimentally). That was considered to be a puzzle [13]. A similar puzzle occurred when niobium was investigated [14–16].

In 1996 Savrasov and Savrasov [17] evaluated $\rho(T)$ and $\alpha^2F(\nu)$ for aluminium, vanadium, tantalum, lead, niobium and molybdenum as well as palladium and copper. Apart from niobium (at $T > 300$ K) and copper, their $\rho(T)$ is lower than the experimental data, significantly so in the case of lead. However their $\alpha^2F(\nu)$ still exceeds experimental values by a factor 2 or 3 in places. To reproduce observed T_c values they were forced to adjust μ^* freely. In the case of vanadium and niobium (resistivity largely correct) they let $\mu^* = 0.30$ and 0.21, instead of the respective tunnelling values 0.15 and between 0.11 and 0.16 [18].

In summary, in numerous attempts over many years values of $\alpha^2F(\nu)$ are always found to be too high when $\rho(T)$ is reasonable (obtained using a pseudopotential from band calculation) or conversely but equivalently $\alpha^2F(\nu)$ reasonable but $\rho(T)$ too low (using a Heine-Abarenkov potential). The import is that somehow the strength of the electron-phonon interaction has to be curtailed in a superconductor.

Aside from these numerical concerns, the BCS theory also has the conceptual difficulty that, in the presence of both normal and umklapp scattering, the occupation probability of electron pair destination states is doubly and contradictorily defined [3, 4]. We introduce an empirical rule to dictate that in a superconductor the electron-phonon interaction does not pair electrons when normal and umklapp scattering compete (though each on its own can lead to superconductivity). This scenario has an exact proof in the BCS theory, see Appendix in [4] which shows that electron pairs cannot form under the circumstances. Superconductivity then arises solely from residual umklapp scattering of pairs (in real crystalline systems normal and umklapp scattering always coexist and the exclusively normal scattering scenario does not arise). In a series of publications we proved the validity of this empirical rule: it allows consistent potentials for the electron-phonon interaction to be used to evaluate both normal state electrical resistivity and superconducting tunnelling conductance with high accuracy in lead, aluminium, niobium and tantalum [3, 4] as well as in tungsten, iridium, molybdenum and vanadium [19, 20].

III. LEAD: LATTICE DISPERSION

Our procedure starts with phonon dispersion calculations. We pay some attention to lead phonons. In addition to the brief review of the topic in [19] we wish to mention an interesting episode showing how far involved investigators are willing to go in order to get to the bottom of the problem. In 1989 Chen and Overhauser named lead as one of the most complicated members of the simple-metal group, posing a challenge for more than 25 years up till then [22]. Suggested explanations in the literature included a third-order perturbation correction to the electron-ion pseudopotential, conduction-electron-core exchange, nonlocal pseudopotentials, relativistic spin-orbit interaction and effective electron-mass

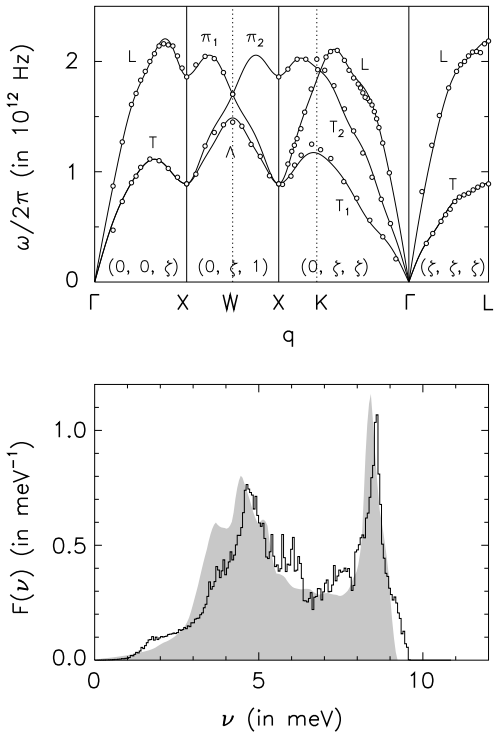

FIG. 1: Lead phonon properties. Upper: Frequency dispersion from neutron scattering by Brockhouse et al (open circles) and calculation (continuous curve), usual (fcc) reciprocal site conventions. Lower: Frequency distribution from neutron scattering by Stedman et al (grey silhouette) and current calculation (histogram).

TABLE I: ATOMIC FORCE CONSTANTS OF LEAD[a]

Site[b]	XX	YY	ZZ	XY	XZ	YZ
(1, 1, 0)	4.2968	4.2968	-2.1348	4.2968		
(2, 0, 0)	1.0331	-0.3902	-0.3902			
(2, 1, 1)	0.0655	0.0640	0.0640	0.0433	-0.0433	-0.0217
(2, 2, 0)	0.9091	0.9091	0.8587	0.9091		
(3, 1, 0)	-0.7909	-0.0551	0.0369	-0.2538		
(2, 2, 2)	0.0485	0.0485	0.0485	0.0415	-0.0415	-0.0415
(3, 2, 1)	-0.0490	-0.1090	-0.1449	-0.0625	0.0313	0.0208
(4, 0, 0)	1.0401	-0.0272	-0.0272			
(4, 1, 1)	0.1078	0.0325	0.0325	0.0323	-0.0323	-0.0081
(4, 2, 0)	0.0302	0.1719	0.2191	0.0809		
(3, 3, 2)	0.2143	0.2143	0.0991	0.2131	-0.1420	-0.1420
(4, 2, 2)	-0.3560	-0.1125	-0.1125	-0.1832	0.1832	0.0916
(4, 3, 1)	0.0931	-0.0444	-0.2015	0.0315	-0.0105	-0.0079
(5, 2, 1)	-0.2048	0.0486	0.0848	-0.0561	0.0280	0.0112
(4, 4, 0)	0.0735	0.0735	0.0888	0.0735		
(4, 3, 3)	-0.0852	0.0156	0.0156	-0.0703	0.0703	0.0527
(4, 4, 2)	0.0853	0.0853	-0.0157	0.0908	-0.0454	-0.0454
(5, 3, 2)	0.0022	-0.0024	-0.0039	-0.0004	0.0003	0.0002
(6, 2, 0)	0.0229	0.0150	0.0140	0.0113		
(5, 4, 1)	0.0236	0.0155	0.0020	0.0191	-0.0048	-0.0038

[a] in newton/m
[b] in 1/2 crystal constant

corrections [22]. Furthermore Chen and Overhauser were not convinced that Fermi surface distortion, or inapplicability of the usual plane wave presentation of the electron gas ground state, could be the answer [22].

According to Chen and Overhauser the challenge of the lead phonons lies mostly in the significant frequency dip in both the longitudinal and transverse modes towards the (0, 0, 1) zone-boundary point [22]. They believed the reason lay in the so-called spin-density waves that justified the introduction of a 6×6 dynamic matrix to replace the 3×3 matrix in the Born-von Kármán model. The Chen-Overhauser matrix depends on a parameter, A, adjustable for data fitting [22]. Unfortunately an experiment in 1992 by Overhauser and Giebuttowicz was unable to demonstrate that spin-density waves were relevant to explaining lead phonon dispersion [23].

Brockhouse et al had suggested that the interatomic forces in lead are of long range and sometimes of alternating sign and they reached a pessimistic conclusion that it is not possible to obtain a detailed description of the force constants within the Born-von Kármán theory [24]. Chen and Overhauser rejected the long-range-force explanation nominally for the reason that it overlooks some small features in the dispersion curves [22] but apparently were also motivated by their intention to calculate lead phonons with the 6×6 dynamic matrix. Indeed it does not appear to be an easy task to take care of the many peculiar features of lead phonon data, shown as open circles in the upper part of FIG. 1, with the 3×3 Born-von Kármán matrix.

We test the suggestion of Brockhouse in order to leave no stone unturned within the simplest theory. We determine the force constants in the Born-von Kármán theory over 20 neighbour atomic shells. Previously we selectively sampled the comprehensive neutron scattering data for lead by Stedman, Almqvist and Nilsson [25] along the high symmetry directions of the metal. We achieved a good fit between theory and these selected data [19]. We observed a 0.3 meV shift of the longitudinal peak of the theoretical phonon density of states against the experimental peak, together with a similar mismatch between the theoretical and experimental peaks of $\alpha^2 F(\nu)$ [19]. We suspect that the sampled neutron data may not be sufficiently representative.

Now we follow the same approach to fit the neutron scattering data of Brockhouse et al that were measured specifically in the directions of high symmetry of lead single crystals [24]. For the convenience of the reader we outline our procedure of calculation. We employ a central force model with 40 adjustable parameters for 20 neighbouring atomic shells [26]. We compare Born-von Kármán calculation and experimental measurement at the 104 (36 previously) sample phonon frequencies tabled in [24] too numerous for a least square fitting but presenting no difficulty when we follow the algorithm of Hooke and Jeeves [27]. In the pattern search phase of the algorithm the 40 parameters are perturbed in turn.

A perturbation is registered as positive if it improves fitting between calculation and measurement, otherwise it is registered as negative. In the pattern move phase all the positive perturbations are performed simultaneously, negative perturbations are performed simultaneously in the opposite directions, to the extent needed for best fitting. This is repeated until the fit no longer improves.

In the upper part of FIG. 1 we show the result of calculation as continuous curves. We see that the significant dips of both the longitudinal (L) and transverse (T) branches of the dispersion curves in the $(0, 0, \zeta)$ direction towards the Brillouin zone boundary, marked by X, are fitted well. Numerous other small features of the curves are also fitted well, including the minor dip in the ΓK section of the L branch in the $(0, \zeta, \zeta)$ direction, thought to arise from the Kohn effect. In the $(0, \zeta, 1)$ direction (XWX) the Λ branch does not cross the π_1 and π_2 branches. It is interesting that in [24] these branches, apparently from hand drawing to guide the eye, do cross each other. This hand drawing can be found in popular text books, see page 441 of [28].

The phonon frequency distribution is defined as:

$$F(\nu) = \frac{1}{N} \sum_{\mathbf{q},\ell} \delta(\nu - \hbar\omega_\ell) \tag{1}$$

where N is the number of atoms in a unit volume, $\mathbf{q}$ runs over the first phonon Brillouin zone, $\omega_\ell = \omega_\ell(\mathbf{q})$ is the phonon frequency and ℓ identifies polarisation [19]. In Eq. (1) the delta function tells us that the phonons are counted with respect to their energy (frequency) and so we have to convert the summation over $\mathbf{q}$ into an integration over ω_ℓ. To this end we have to evaluate $dq/d\omega_\ell$ from phonon dispersion knowledge. We refrain from differentiating numerically the phonon dispersion curves in the upper part of FIG. 1 because that is prone to substantial numerical errors and probably is the reason for the significant longitudinal peak of the lead $F(\nu)$ in for example [29]. Instead we count contributions to $F(\nu)$ by lead phonons once the value of ω_ℓ falls into a destined section of a grid of discrete values of ν [26].

In the lower part of FIG. 1 we compare the experimental phonon density of states from [25] with our calculation. Now the theoretical and experimental longitudinal peaks are much closer compared with those in [19]. In TABLE I we list values of the atomic force constants. They are largely similar to the force constants tabled in [19] though they do not exhibit a clear tendency to cut off beyond the 17th shell. We are warned that in lead a good fit in the directions of high symmetry may not ensure good enough fit in other directions, as we are going to see from the following Sections. An early pointer to this issue can be found in [30].

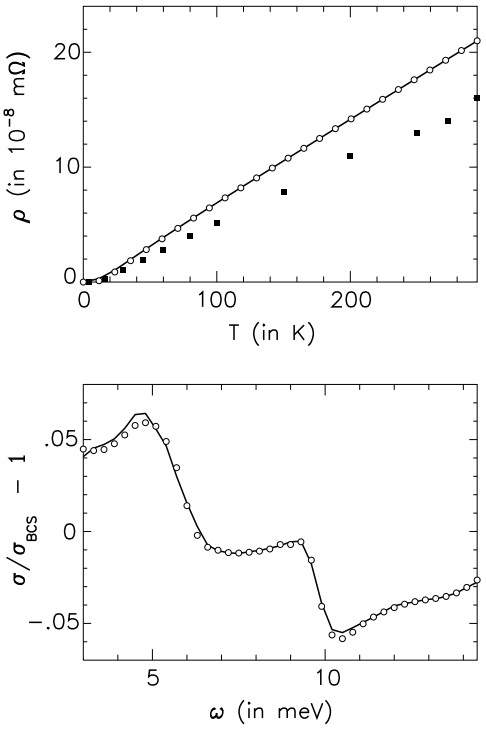

FIG. 2: Upper: Lead electrical resistivity from experiment (curve), current calculation (open circles) and Tomlinson-Carbotte calculation (filled squares). Lower: Lead superconducting tunnelling conductance from experiment (curve) and current calculation (open circles).

IV. LEAD: ELECTRON-PHONON INTERACTION

We calibrate the strength of the electron-phonon interaction in lead with measured values of $\rho(T)$ in the normal state. In formulation $\rho(T)$ is determined by the electron-phonon transport spectral density that by definition is of the following form:

$$\alpha^2 F_{\rm tr}(\nu) = \frac{1}{N} \sum_{\mathbf{q},\ell} \delta(\nu - \hbar\omega_\ell)\delta(\epsilon - \epsilon_F) \frac{\mathbf{k}\cdot\mathbf{q}}{\mathbf{k}\cdot\mathbf{k}} \, |g_\ell(\mathbf{q})|^2 \tag{2}$$

where $\mathbf{q} = \mathbf{k}' - \mathbf{k}$ is the phonon vector momentum, $\mathbf{k}$ and $\mathbf{k}'$ initial and end momenta of the electron, $\epsilon = \epsilon(\mathbf{k}')$ the energy of the scattered electron,

$$g_\ell(\mathbf{q}) = \sqrt{\frac{\hbar}{2M\omega_\ell}} \, \mathbf{e}_\ell \cdot \langle \psi_{\mathbf{k}} | \nabla V | \psi_{\mathbf{k}'} \rangle \tag{3}$$

measures the strength of the electron-phonon interaction, with M being mass of the atom, $\mathbf{e}_\ell$ phonon polarisation vector, $\psi_{\mathbf{k}}$ and $\psi_{\mathbf{k}'}$ initial and end wavefunctions of the electron [19]. We assume a muffin-tin pseudopotential so that

$$V(r) = \delta V \cos\left(\frac{\pi r}{2r_1}\right) \tag{4}$$

within a constant value when $0 < r < r_1$, otherwise it assumes that constant value, δV and r_1 measure the depth and width of the potential well. A programmable version of Eq. (3) can be found in [19] where we have removed differentiation upon $V(r)$ with the technique of integration by parts.

In Eq. (2) $\alpha^2 F_{\rm tr}(\nu)$ is anisotropic, due to its dependence on $\mathbf{k}$. It becomes isotropic if we assume a spherical Fermi surface and we have good reasons to do so. We follow Carbotte and Dynes to include umklapp scattering in evaluating $\rho(T)$ [31]. We run $\mathbf{q}$ over a sphere of radius $2k_F$ that conceptually envelops the entire Fermi surface, k_F being the scalar Fermi momentum. This practice is far from the physical reality that, owing to the exclusion principle, the electron-phonon interaction takes place nowhere but over the Fermi surface [32]. It totally disregards topology of the Fermi surface, saving that all the possible phonon states have been covered, but with good numerical accuracy in $\alpha^2 F(\nu)$. Furthermore in Eqs. (2) and (3) there is trade-off between the values of $\mathbf{k}$ and $V(r)$. If the simple pseudopotential in Eq. (4) turns out to be good enough to fit theoretical and experimental $\rho(T)$ accurately, with a spherical Fermi surface, then we have to admit that we have little reason to elaborate the shape of the surface any further.

We proceed by assuming a spherical Fermi surface and determine $V(r)$ in Eq. (4) via inversion. We start with a proxy experimental $\rho(T)$, generated by the Bloch-Grüneison formula with high accuracy [33], and seek best agreement between theory and that experimental data by varying δV and r_1 in Eq. (4) via a simple computer program. We find that when $\delta V = -3.008$ (in units of Fermi energy) and $r_1 = 0.802$ (in units of crystal constant) on average the deviation is 0.15% (against ρ at 295 K). In the upper part of FIG. 2 we show graphically the theoretical (curve) and experimental (open circles) $\rho(T)$ over $0 \le T \le 295$ K. We also show $\rho(T)$ found by Tomlinson and Carbotte (solid squares) for comparison [6].

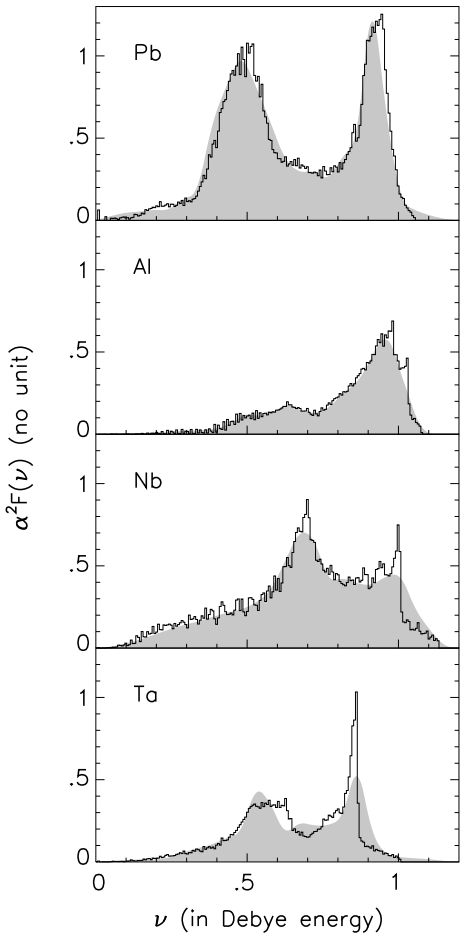

FIG. 3: Electron-phonon spectral densities in metallic superconductors from experiment (grey silhouettes) and current calculation (histograms).

V. LEAD: NUMERICAL PAIRING SCHEME

In the BCS-Eliashberg-Nambu formalism the tunnelling conductance of a superconductor is determined by the following electron-phonon spectral density:

$$\alpha^2 F(\nu) = \frac{1}{N} \sum_{\mathbf{q},\ell} \delta(\nu - \hbar\omega_\ell)\delta(\epsilon - \epsilon_F) S(\mathbf{q}) |g_\ell(\mathbf{q})|^2 \quad (5)$$

which resembles Eq. (2) closely [19]. In Eq. (5) we have placed a survival rate factor, $S(\mathbf{q})$, which in accordance with our empirical rule [3, 4] is defined as follows:

$$S(\mathbf{q}) = \begin{cases} 0, & \text{if } \mathbf{k}' \pm \mathbf{k} \text{ is in BZ} \\ 1/2, & \text{otherwise} \end{cases} \quad (6)$$

where $\mathbf{q} = \mathbf{k}' - \mathbf{k}$ and BZ stands for the first phonon Brillouin zone. The $\mathbf{k}' \pm \mathbf{k}$ term arises from consideration of scattering from both members of the Cooper pair, in initial states $\mathbf{k}$ and $-\mathbf{k}$, to a final state $\mathbf{k}'$. We assume a spherical Fermi surface, following our treatment of Eq. (2), so that in Eq. (5) $\alpha^2 F(\nu)$ becomes isotropic. In this case and with Debye phonons (spherical BZ) we have $S(\mathbf{q}) = 0$ if $q < q_D$ or $4k_F^2 - q^2 < q_D^2$, otherwise $S(\mathbf{q}) = 1/2$, q_D stands for Debye momentum. The resulting empirical survival rate is shown as the grey rectangles in FIG. 4.

Now we wish to verify whether this empirical survival rate in Eq. (6) could arise naturally from physics. We seek a numerical version of $S(\mathbf{q})$ without *a priori* restrictions to its values apart from a symmetry requirement. Let $(\mathbf{k}, -\mathbf{k})$ and $(\mathbf{k}', -\mathbf{k}')$ be the initial and end states of a Cooper pair (spin absorbed into $\mathbf{k}$) and $h(\mathbf{k}')$ and $h(-\mathbf{k}')$ electron occupation probabilities at $\mathbf{k}'$ and $-\mathbf{k}'$. By symmetry we must have $h(\mathbf{k}') = h(-\mathbf{k}')$. Consequently we require $S(\mathbf{k}') = S(-\mathbf{k}')$ or $S(\mathbf{q_1}) = S(\mathbf{q_2})$, where $\mathbf{q_1} = \mathbf{k}' - \mathbf{k}$ and $\mathbf{q_2} = -\mathbf{k}' - \mathbf{k}$. We further assume $S(\mathbf{q_1}) =$

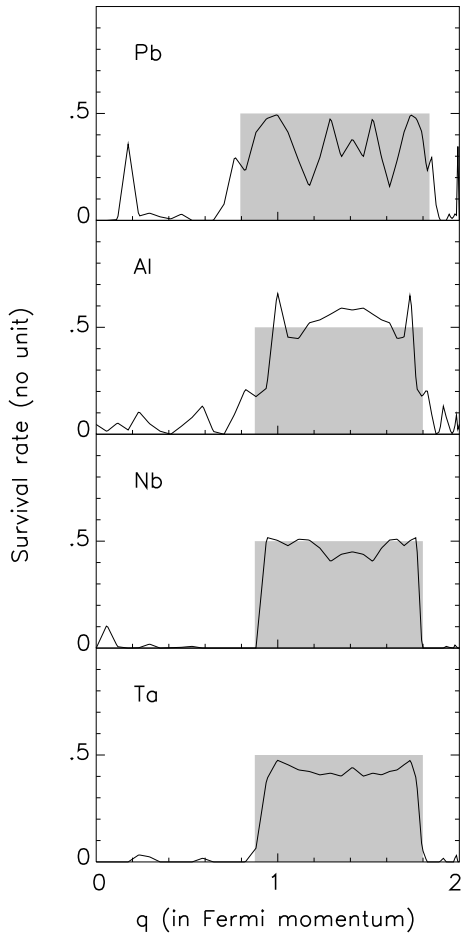

FIG. 4: The survival rate of the electron-phonon interaction in metals defined by the empirical rule assuming spherical Fermi surface and Debye phonons (silhouette) and the explicitly calculated values (curves).

$S(q_1) = S(|\mathbf{k}' - \mathbf{k}|)$ and $S(\mathbf{q_2}) = S(q_2) = S(|\mathbf{k}' + \mathbf{k}|)$. This implies a more strict constraint upon $S(\mathbf{q})$ because now some information carried by $\mathbf{q}$ has been stripped off. We are going to show that we do not have to relax this constraint in order to achieve a good fit between theory and experiment.

In determining $S(q)$ numerically we start from the experimental values of superconducting tunnelling conductance in lead, σ, shown as the continuous curve in the lower part of FIG. 2 [34]. For a spherical Fermi surface the maximum value of q is $2k_F$. We seek values of $S(q)$ over a grid of 25 equal divisions between $q = 0$ and $1.414k_F$ (scattering angle = 90°). Other values of $S(q)$ are found from symmetry against scattering angle and interpolation between mesh points. Initially we let $S(q)$ assume the shape of the grey rectangles in FIG. 4 demonstrating the empirical rule. This $S(q)$ leads through Eq. (5) to $\alpha^2F(\nu)$ that in turn leads to theoretical values of tunnelling conductance [19]. To refine the calculated conductance we apply the Hooke-Jeeves algorithm to adjust $S(q)$ and eventually reach a good fit of calculated conductance shown as open circles to the measured values in the lower part of FIG. 2; here the average deviation between observation and computation is a mere 0.18% with respect to the average value of σ so there is little further benefit in replacing the scalar argument of $S(q)$ with a vector. En route we also find the theoretical $\alpha^2F(\nu)$ in lead shown as a histogram in FIG. 3. The experimental $\alpha^2F(\nu)$, evaluated in house from the experimental σ, is also shown for comparison as a grey silhouette in FIG. 3.

In FIG. 4 we show the numerically optimised $S(q)$. We deduce that the zigzag shape is not due to low numerical resolution because some seemingly straight sections run across a number of the grid intervals. By and large the numerical $S(q)$ for Pb in FIG. 4 is tolerably well enveloped by the empirical grey rectangle for a spherical Fermi surface and Debye phonons. The zigzag deviations indicate some remaining inaccuracy in our analysis, possibly in the lead phonon dispersion away from the directions of high symmetry.

VI. ALUMINIUM, NIOBIUM AND TANTALUM

For purposes of comparison we turn our attention to some other examples. Aluminium phonons are discussed in [26]. High quality tunnelling conductance data from aluminium are not available, mainly because the superconductor has a relatively low T_c (1.2 K) [35]. Giaever measured tunnelling conductance from an $Al/Al_2O_3/Pb$ junction in 1960 but without sufficient resolution to allow further investigation [36]. Moshe Dayan measured crystalline and granular Al in 1978 and extracted $\alpha^2F(\nu)$ [37]. Zasadzinski, Burnell, Wolf and Arnold measured an M-Al_2O_3-Al/V proximity structure and extracted $\alpha^2F(\nu)$ for both aluminium and vanadium [38]. Khim measured an Al/Pb proximate junction in 1979 and extracted $\alpha^2F(\nu)$ (grey silhouette in FIG. 4) but did not publish the tunnelling data [39, 40]. From the Khim $\alpha^2F(\nu)$ data we find the superconducting energy gap function via the BCS-Eliashberg-Nambu equation which in turn leads via the formula in for example [19] to the aluminium tunnelling conductance we need as experimental input.

In aluminium we find that to obtain a good fit in the $\rho(T)$ inversion we have to assume a Gaussian form for the atomic pseudopotential:

$$V(r) = \delta V \exp\left[-\left(\frac{r}{r_1}\right)^2\right] \tag{7}$$

with $\delta V = -2.716$ (in Fermi energy) and $r_1 = 0.433$ (in crystal constant). The proxy experimental resistivity was derived from the Bloch-Grüneison formula [33], $0 \leq T \leq 295$ K and the average deviation was 0.90% relative to ρ at 295 K. The above Gaussian potential leads to

the $S(q)$ shown in FIG. 4, giving a relatively mild zigzag compared with the case of lead. Probably the detailed $S(q)$ structure is due to inaccuracies in the experimental aluminium tunnelling conductance. Overall it compares tolerably well with the empirical $S(q)$ shown in FIG. 4 as the grey rectangle. The numerical $\alpha^2F(\nu)$ in FIG. 3 (histogram) agrees well with the experimental values (silhouette).

Niobium phonons are discussed in [19], resistivity is discussed in [41] and tunnelling conductance reported in [42]. These lead to $\delta V = -4.142$ (in Fermi energy) and $r_1 = 1.045$ (in crystal constant) in Eq. (4) giving numerical $\rho(T)$ over $0 \leq T \leq 285$ K with a deviation of 0.23% relative to ρ at 295 K. Consequently we find $S(q)$ in FIG. 4 (curve) fits well to its empirical values (rectangle). The numerical $\alpha^2F(\nu)$ in FIG. 3 (histogram) agrees well with experimental values (silhouette).

Tantalum phonons are discussed in [43], experimental resistivity is from the Bloch-Grünison formula [33] and tunnelling conductance is reported in [39]. These lead to $\delta V = -4.542$ (in Fermi energy) and $r_1 = 1.058$ (in crystal constant) in Eq. (4) giving numerical $\rho(T)$ over $0 \leq T \leq 285$ K with a deviation of 0.54% relative to ρ at 295 K. Consequently we find the numerical $S(q)$ in FIG. 4 (curve) fits well to its empirical values (rectangle). Again, the numerical $\alpha^2F(\nu)$ in FIG. 3 (histogram) agrees well with experimental values (silhouette).

VII. DISCUSSION

In our empirical pairing scheme, expressed in analytical form in Eq. (6), the survival rate of the pairing interaction is determined by the vector wavenumber, $\mathbf{q}$, that depends on both the frequency of vibration and direction of propagation of the phonons. In the previous two sections we have replaced $\mathbf{q}$ with q and therefore removed the effect of phonon direction from consideration. This is a model chosen for simplicity but it is clear from the spectral densities in FIG. 3 that it achieves high accuracy. The message is that in calculating superconducting properties from first principles the dominant concern should be to find to what extent the electron-phonon interaction survives to pair electrons in the superconducting state, rather than searching for example for some subtlety in the highly sophisticated topology of the Fermi surface.

Our empirical pairing scheme, in the form of Eq. (6), is extremely simple. At present it is not entirely clear what is the exact physical reason or reasons for it to arise. However it is apparent from FIG. 4 that there must be a lot of truth in Eq. (6). The numerical outcome of Eq. (6), with more or less zigzagging (strongly in the case of lead), is always enveloped reasonably well by the empirical version of Eq. (6) (grey rectangles). These curves evolve automatically from computation, with pairing symmetry as the only constraint, in the search for a good fit to the tunnelling conductance data shown for example in the lower part of FIG. 2. They are straightforward and provide objective answers to the question: to what extent should the electron-phonon interaction be curtailed in order to reproduce the experimental tunnelling conductance within the BCS-Eliashberg-Nambu theory? There is little, if any, *a priori* judgement and/or uncontrolled approximation required when the curves in FIG. 4 are generated.

In FIG. 4 the curves compare well with the grey rectangles in niobium and tantalum but somewhat less so in aluminium and lead. The lead problem may lie in the well-known difficulty in phonon dispersion calculations. Although in FIG. 1 the calculated dispersion curve in lead fits experimental sample data well in a few directions of high symmetry, there is no guarantee of similar good fitting in other directions. The aluminium problem on the other hand is thought to arise from deficiencies in the tunnelling measurements made difficult by the low transition temperature of the metal.

VIII. CONCLUSIONS

There is little doubt that the BCS theory needs to be overhauled. The empirical (grey rectangles) and numerical (curves) survival rates in FIG. 4 tell us exactly how significantly contributions from the electron-phonon interaction in the normal state have to be curtailed in order to achieve a good fit between theory and observation in the superconducting state in lead, aluminium, niobium and tantalum and therefore overhaul the BCS theory. This survival rate is little more than a quantitative and accurate reflection of the Mott-Jones theory of electrical resistivity and BCS theory of superconductivity. Little *a priori* conceptual judgement and/or numerical approximation has been involved. There is no room for a measure such as adjusting the Coulomb pseudopotential μ^* without justification to reconcile the BCS theory with the normal state electron-phonon interaction without the survival rate considerations. This is especially relevant and perhaps helpful and timely in light of the recent discovery of $T_c = 203$ K at high pressures in the sulfur hydride system [44–48].

[1] J. Bardeen, L.N. Cooper, J.R. Schrieffer, *Phys. Rev.* **108** (1957) 1175.
[2] J.E. Hirsch, *Phys. Scr.* **80** (2009) 035702.
[3] X.H. Zheng, D.G. Walmsley, *Solid State Commun.* **192** (2014) 56.
[4] X.H. Zheng, D.G. Walmsley, *Phys. Scr.* **89** (2014) 095803.
[5] P.G. Tomlinson, J.P. Carbotte, *Phys. Rev. B* **13** (1976) 4738.
[6] P.G. Tomlinson, J.P. Carbotte, *Can. J. Phys.* **55** (1977)

751.
[7] A. Eiling, J.S. Schiling, *J. Phys. F: Metal Phys.* **11** (1981) 623.
[8] C.R. Leavens, J.P. Carbotte, *Ann. Phys.* **70** (1972) 338.
[9] P.T. Truant, J.P. Carbotte, *Can. J. Phys.* **52** (1974) 618.
[10] H.K. Leung, J.P. Carbotte, C. R. Leavens, *J. Low Temp. Phys.* **24** (1976) 25.
[11] M. Peter, J. Ashkenazi, M. Dacorogna, *Helv. Phys. Acta* **50** (1977) 267.
[12] D. Glötzel, D. Rainer, H.R. Schober, *Z. Physik* **35** (1979) 317.
[13] A. Al-Lehaibi, J.C. Swihart, W.H. Butler, F.J. Pinski, *Phys. Rev. B* **36** (1987) 4103.
[14] W.H. Butler, H.G. Smith, N. Wakabayashi, *Phys. Rev. Lett.* **36** (1977) 1004.
[15] W.H.Butler, F. Pinski, P.B. Allen, *Phys. Rev. B* **19** (1979) 3708.
[16] F.J.Pinski, P.B. Allen, W.H. Butler *Phys. Rev. B* **23** (1981) 5080.
[17] S.Y. Savrasov, D.Y. Savrasov, *Phys. Rev. B* **54** (1996) 16487.
[18] B. Mitrović, H.G. Zarate, J.P. Carbotte, *Phys. Rev. B* **29** (1984) 184 .
[19] X.H. Zheng, D.G. Walmsley, *Physica C* **506** (2014) 100.
[20] X.H. Zheng, D.G. Walmsley *Physica C* **515** (2015) 41.
[21] J.P. Carbotte, *Rev. Modern Phys.* **62** (1990) 1027.
[22] X.M. Chen, A.W. Overhauser, *Phys. Rev. B* **39** (1989) 10570.
[23] A.W. Overhauser, T.M. Giebultowicz, *Phys. Rev. B* **47** (1993) 14338.
[24] B.N. Brockhouse, T. Arase, G. Caglioti, K.R. Rao, A.D.B. Woods, *Phys. Rev.* **128** (1962) 1099.
[25] R. Stedman, L.Almqvist, G. Nilson, *Phys. Rev.* **162** (1967) 549.
[26] X.H. Zheng, D.G. Walmsley *J. Low Temp. Phys.* **166**(2012) 279.
[27] R. Hooke, T.A. Jeeves, *J. Assoc. Comput. Math.* **8** (1961) 212.
[28] N.W. Ashcroft, N.D. Mermin, *Solid state physics* Saunders, New York, 1976.
[29] E.R. Cowley, *Solid State Commun* **14** (1974) 587.
[30] R.C.Dynes, J.P. Carbotte, E.J. Woll Jr, *Solid State Commun.* **6** (1968) 101.
[31] J.P. Carbotte, R.C.Dynes *Phy. Rev.* **172** (1968) 476.
[32] N.F. Mott, H. Jones, *The theory of the properties of metals* Dover, New York, 1958.
[33] J. Ziman, *Electrons and phonons* Clarendon, Oxford, 2001.
[34] W.L. McMillan, J.M. Rowell, *Phys. Rev. Lett.* **181** (1965) 108.
[35] B.L. Blackford, R.H. March, *Can. J. Phys.* **46** (1967) 141.
[36] I. Giaever, 1960 *Phys. Rev. Lett.* **5** (1960) 147.
[37] M. Dayan, *J. Low Temp. Phys.* **32** (1978) 643.
[38] J. Zasadzinski, D.M.Burnell, E.L. Wolf, G.B. Arnold, *Phys. Rev. B* **3** (1982) 1622.
[39] E.L. Wolf, *Principles of electron tunneling spectroscopy* Oxford University Press, Oxford, 1985.
[40] E.L. Wolf, R.J. Noer, D. Burnell, Z.G. Khim, G.B. Arnold, *J. Phys. F: Metal Phys.* **11** (1981) L23.
[41] G.W. Webb, *Phys. Rev.* **181** (1968) 1127.
[42] Z.G. Khim, D. Burnell, E.L. Wolf, *Solid State Commun.* **39** (1981) 159.
[43] X.H. Zheng, D.G. Walmsley, *J. Low Temp. Phys.* **173** (2013) 120.
[44] A.P. Drozdov, M.I. Eremets, I.A. Troyan, V. Senofontov, S.I. Shylin, *Nature* **525** (2015) 73.
[45] Y. Li, J. Hao, H. Liu, Y. Li, Y. Ma, *J. Chem. Phys.* **140** (2014) 174712.
[46] A. Durajski, R. Szczęśniak, Y. Li, *Physica C* **515** (2015) 1.
[47] R. Akashi, M. Kawamura, S. Tsuneyuki, Y. Nomura, R. Arita, *Phys. Rev. B* **91** (2015) 224513.
[48] A. P. Durajski, R. Szczęśniak, L. Pietronero, *Ann. Phys.* DOI 10.1002/andp.201500316 (2015) 1.